Title

Drosophila model to clarify the pathological significance of OPA1 in autosomal dominant optic atrophy

Authors

Yohei Nitta[1,7], Jiro Osaka[2,7], Ryuto Maki[2], Satoko Hakeda-Suzuki[2,3], Emiko Suzuki[4,5], Satoshi Ueki[6], Takashi Suzuki[2] and Atsushi Sugie[1 *]

[1] Brain Research Institute, Niigata University, Niigata, 951-8585, Japan

[2] School of Life Science and Technology, Tokyo Institute of Technology, Yokohama, 226-8501, Japan

[3] Research Initiatives and Promotion Organization, Yokohama National University, Yokohama, 240-8501, Japan

[4] Department of Biological Sciences, Graduate School of Science, Tokyo Metropolitan University, Hachioji 192-0397, Japan

[5] Department of Gene Function and Phenomics, National Institute of Genetics, Mishima, 411-8540, Japan

16 [6] Division of Ophthalmology and Visual Science, Graduate School of Medical and Dental Sciences,

17 Niigata University, Niigata, 951-8585, Japan

18 [7] Equal contribution

19 [*] Corresponding author: atsushi.sugie@bri.niigata-u.ac.jp (A.S.) Tel (+81) 25-227-0616.

20

21

22 **Abstract**

23 Autosomal dominant optic atrophy (DOA) is a progressive form of blindness caused by degeneration

24 of retinal ganglion cells and their axons, mainly caused by mutations in the OPA1 mitochondrial

25 dynamin *like* GTPase (*OPA1)* gene. *OPA1* encodes a dynamin-like GTPase present in the

26 mitochondrial inner membrane. When associated with OPA1 mutations, DOA can present not only

27 ocular symptoms but also multi-organ symptoms (DOA plus). DOA plus often results from point

28 mutations in the GTPase domain, which are assumed to have dominant negative effects. However, the

29 presence of mutations in the GTPase domain does not always result in DOA plus. Therefore, an

30 experimental system to distinguish between DOA and DOA plus is needed. In this study, we found

31 that loss-of-function mutations of the *dOPA1* gene in *Drosophila* can imitate the pathology of optic

32 nerve degeneration observed in DOA. We successfully rescued this degeneration by expressing the

human *OPA1* (*hOPA1*) gene, indicating that *hOPA1* is functionally interchangeable with *dOPA1* in the fly system. However, we could not rescue any previously reported mutations known to cause either DOA or DOA plus. By expressing both WT and DOA plus mutant *hOPA1* forms in the optic nerve of *dOPA1* mutants, we observed that DOA plus mutations suppressed the rescue, facilitating the distinction between loss-of-function and dominant negative mutations in *hOPA1*. The fly model developed in this study can assist in the differential diagnosis between DOA and DOA plus and inform early treatment decisions in patients with mutations in *hOPA1*.

Introduction

Autosomal dominant optic atrophy (DOA) is a progressive form of blindness characterized by selective degeneration of retinal ganglion cells (RGCs) and the axons that form the optic nerve. Despite being a rare disease with a frequency of 1/12,000 to 1/50,000, DOA is the most commonly diagnosed form of hereditary optic neuropathy. In 2000, *OPA1 mitochondrial dynamin like GTPase (OPA1)* was identified as the causative gene for DOA (Alexander et al., 2000; Delettre et al., 2000).

OPA1 encodes a dynamin-like GTPase located in the inner mitochondrial membrane (Olichon et al., 2002). It has various functions, including mitochondrial fusion, mtDNA maintenance, control of cell death, and resistance to reactive oxygen species (ROS) (Lenaers et al., 2021). The most

50 common pathogenic mutation in *OPA1* is the c.2708_2711 delTTAG deletion (Toomes et al., 2001).
51 Five pathogenic mutations, including the one above, result in a substantial decrease in OPA1 protein
52 in the fibroblasts from affected patients (Zanna et al., 2008), supporting the theory that DOA is caused
53 by haploinsufficiency.

54 Optic atrophy is a characteristic feature of *OPA1*-associated DOA; however, multisystem
55 symptoms have been reported in up to 20% of *OPA1* mutation carriers (Yu-Wai-Man et al., 2010a).
56 This is called DOA plus. DOA plus can include sensorineural deafness (Amati-Bonneau et al., 2008),
57 multiple sclerosis (Verny et al., 2008; Yu-Wai-Man et al., 2016), parkinsonism and dementia (Carelli
58 et al., 2015; Lynch et al., 2017), and cardiomyopathy (Spiegel et al., 2016). The R445H mutation is a
59 well-known mutation associated with DOA plus (Amati-Bonneau et al., 2008, 2003; Shimizu et al.,
60 2003). The proportion of mutated OPA1 locations differs between patients with DOA and DOA plus.
61 Missense mutations in the dynamin-featured structure, especially the GTPase domain of *OPA1*, are
62 more likely to cause severe symptoms compared with loss-of-function (LOF) mutations such as
63 deletions or splice site mutations (Yu-Wai-Man et al., 2010a). This is probably due to the dominant
64 negative effect (DN) of a DOA plus mutation on the normal *OPA1* allele, since OPA1 functions as a
65 homo-oligomer (Frezza et al., 2006; Olichon et al., 2006); in fact, its yeast ortholog, Mgm1, forms
66 oligomers, increasing the GTPase activity (Meglei and McQuibban, 2009; Rujiviphat et al., 2009).
67 Particularly, the dynamin-featured structure accounts for 70% of the 233 pathogenic variants of DOA

68 and DOA plus described in the locus-specific database (Ferré et al., 2015). However, mutations in
69 these domains do not determine DOA plus, as it affects only 20% of all *OPA1* mutation carriers. Thus,
70 experimental models to determine whether a gene mutation is LOF or DN are required to distinguish
71 between DOA and DOA plus. Although currently there is no effective treatment for DOA or DOA
72 plus, distinguishing between them allows earlier planning of interventions such as hearing aids, rather
73 than relying solely on visual aids, necessary only for those with DOA plus.

74 As *OPA1* is conserved in various species, DOA models have been reported in vertebrates
75 such as mice and zebrafish, simple organisms such as nematodes and fruit flies, and *in vitro* yeast and
76 cultured cell models (Del Dotto and Carelli, 2021). In mouse models, focal RGC axons decrease in
77 number with mitochondrial abnormalities at the electron microscope level, but the phenotype appears
78 slowly, not allowing for analysis in a short time frame (Alavi et al., 2007; Davies et al., 2007; Nguyen
79 et al., 2011; Sarzi et al., 2012). Zebrafish models have displayed developmental delays in eyes and
80 heads, short length, and body axis abnormalities (Eijkenboom et al., 2019; Rahn et al., 2013) but have
81 not been used to investigate optic nerve degeneration.

82 In *C. elegans*, most studies focused on muscle cells using mutants of *eat-3*, an *OPA1*
83 homolog (Kanazawa et al., 2008; Rolland et al., 2009). However, the mitochondria in the posterior
84 lateral microtubule neurons did not show any difference in size from its wild-type (WT) counterparts

85 (Byrne et al., 2019). Thus, LOF of *eat-3* may have a limited impact on phenotypic outcomes in the
86 nervous system. Nevertheless, a DOA model in which *hOPA1*^{K301A} is expressed in GABAergic motor
87 neurons, showed a decreased number of mitochondria in those cells (Zaninello et al., 2020). In a fly
88 model, the *dOPA1* somatic clone in the eye exhibited a rough-eye phenotype, eye structural
89 abnormalities, and increased MitoSOX fluorescence, which was partially rescued by vitamin E or
90 SOD1 expression (Yarosh et al., 2008). Heterozygous *dOPA1* mutants showed shortened lifespan,
91 elevated ROS levels, and irregular muscle tissue mitochondrial structures (Tang et al., 2009).
92 Moreover, the Electroretinogram (ERG) pattern showed age-dependent decreases in the on transient
93 response, heart rate, negative geotaxis response, and increased heart arrhythmia due to heat shock
94 stress (Shahrestani et al., 2009). However, except for mice, the evidence of optic nerve axonal
95 abnormalities is limited in model organisms such as zebrafish, worms, and flies.

96 The structure of the *Drosophila* visual system is similar to that of mammals (Sanes and
97 Zipursky, 2010), with conserved mechanisms of synaptogenesis and neural circuit formation (Sanes
98 and Zipursky, 2020). *Drosophila* photoreceptors type R7/8 extend their retinal axons from the retina
99 directly into the brain, forming synapses in the second optic ganglion medulla via the chiasma (Figure
100 1A), having potential application as a model for mammalian photoreceptors and RGCs. Based on this,
101 we aimed to develop an experimental model for observing and quantifying degeneration in the
102 *Drosophila* retinal axon (Nitta et al., 2023; Richard et al., 2022).

103 In this study, a *dOPA1* LOF could mimic the human DOA, in which mitochondrial
104 fragmentation, increased ROS levels, and neurodegeneration occur in retinal axons. The axonal
105 degeneration induced by the *dOPA1* mutant was rescued by the expression of human *OPA1* (*hOPA1*).
106 This demonstrated that the function of *hOPA1* is the same as in the fly. As none of the previously
107 reported mutations known to cause DOA or DOA plus were rescued, their function seems to be
108 impaired. To distinguish between the effect of LOF and DN mutations, we expressed the *hOPA1* gene
109 of both WT and mutation in a genetic background in which *dOPA1* was deleted in retinal axons. The
110 DOA plus mutations D438V and R445H inhibited the rescue by the WT of *hOPA1*. Taken together,
111 we generated a new *Drosophila* DOA model which served to isolate the LOF or DN effect of *hOPA1*
112 mutations.

113

114 **Results**

115 ***dOPA1* depletion caused mitochondrial fragmentation in axon terminals**

116 The OPA1 protein is located in the inner mitochondrial membrane. To confirm whether dOPA1 is also
117 localized in the mitochondria of *Drosophila* retinal axons, we used a Gal4/UAS system (Brand and
118 Perrimon, 1993) and expressed HA-tagged dOPA1 proteins using the eye-specific *GMR-Gal4* driver
119 (Newsome et al., 2000a, 2000b). The outer membrane of the mitochondria was visualized with

120 mCherry-mito, which tagged the transmembrane domain of Miro with mCherry (Vagnoni and Bullock,
121 2016). Confocal microscopy revealed that the HA signals colocalized with mCherry-mito in the axon
122 terminals of photoreceptor cells (Figure 1B). This indicated that dOPA1 colocalizes with mitochondria
123 in retinal axons.

124 To examine the impact of *dOPA1* on mitochondrial structure and density, we analyzed
125 mitochondria in *dOPA1* RNAi flies. The intensity of the mitochondrial signal was significantly
126 reduced in the retinal axons of these flies (Figure 1C and D; quantification in 1E), suggesting a
127 decreased number of mitochondria in retinal axons. However, whether this decrease is due to
128 degradation resulting from a decline in mitochondrial quality or axonal transport failure remains
129 unclear. Previously, impaired mitochondrial transport was reported in the LOF of *marf* (MFN 1/2
130 homolog), which is necessary for the fusion of the outer membrane of mitochondria (Sandoval et al.,
131 2014). Thus, we investigated if the LOF of *dOPA1* may cause transport defects, which may be
132 responsible for the reduced mitochondrial density in retinal axons in *dOPA1* RNAi flies. To this end,
133 we observed the photoreceptor neurons after puparium formation at 24 h, which allowed us to
134 simultaneously visualize the cell bodies and axon terminals of the photoreceptors (Figure S1A). Both
135 *dOPA1* knockdown and control flies showed mitochondrial signals in the axon terminals (Figure S1B
136 and C). However, no mitochondrial signals were observed in the axon terminals of flies with a
137 knockdown of *milton*, which is thought to act as an adaptor between kinesin to mitochondria,

138 promoting anterograde transport (Figure S1D). These findings suggest that trafficking defects are not
139 the main cause of the mitochondrial mislocalization observed in the retinal axons of the *dOPA1*
140 knockdown.

141 Nevertheless, the degradation resulting from mitochondrial fragmentation may have
142 decreased the mitochondrial signal. To further analyze the mitochondrial morphology of retinal axons
143 in the LOF of *dOPA1*, we conducted an electron microscopy analysis (Figure 1F and G). Although
144 *Drosophila* has eight types of photoreceptors, the axons of R1–6, which project to the lamina of the
145 first optic lobe, can be identified without markers; thus, we chose them for this experiment. The *dOPA1*
146 knockdown led to a significant decrease in mitochondria size in R1–6 axons (Figure 1F–H). In addition,
147 there was significant heterogeneity in healthy mitochondria, ranging from dense-matrix (Class A) to
148 swollen mitochondria with a hypodense matrix (Class B) (Figures 1I). Knocking down *dOpa1* in R1–
149 6 axon terminals resulted in severely abnormal mitochondrial ultrastructure (22.8%; Figure 1J). These
150 results suggest that *dOPA1* is involved in maintaining proper mitochondrial morphology by promoting
151 mitochondrial fusion in retinal axons. Previous studies have observed mitochondrial fragmentation in
152 S2 cells (McQuibban et al., 2006), muscle tissue (Deng et al., 2008), segmental nerves (Trevisan et
153 al., 2018), and ommatidia (Yarosh et al., 2008) due to LOF of *dOPA1*, which is consistent with the
154 results observed in the retinal axons.

155 To verify whether ROS is increased in the retinal axons in *dOPA1* knockdown
156 photoreceptors, we measured the ROS levels in the knockdown retinal axons using MitoSOX, a
157 mitochondrial superoxide indicator (Yarosh et al., 2008). The results showed significantly elevated
158 ROS levels in *dOPA1* knockdown retinal axons compared to control (Figure 2A and B; quantification
159 in 2C).

160

161 **The *dOPA1* LOF leads to progressive distal degeneration of *Drosophila* photoreceptors**

162 We tested whether knocking down *dOPA1* causes optic nerve degeneration in *Drosophila*. To this end,
163 we performed an RNAi experiment using the *GMR-Gal4* driver and evaluated the number of retinal
164 axons projecting to the second optic ganglion medulla (Figure 3A). To compare the number of retinal
165 axon terminals–R7 axons–between genotypes, we used a previously developed automated method,
166 MeDUsA (method for the quantification of degeneration using fly axons) (Nitta et al., 2023). Our
167 results showed that the *dOPA1* knockdown caused axonal degeneration one day after eclosion, further
168 decreasing one week later (Figure 3B–E, quantification in 3F). To determine whether the degeneration
169 was limited to the axons, we counted the number of rhabdomeres in the cell bodies. Each compound
170 eye comprises 700–800 ommatidia, with each ommatidium containing eight types of photoreceptors,
171 designated as R1–R8. The distal region of an ommatidium reveals the R1–R7 photoreceptors with a

172 stereotypical arrangement of rhabdomeres (arrowheads in Figure 3G–J). Since it is easy to evaluate
173 retinal degeneration by counting the number of rhabdomeres, a decrease in their number indicates
174 degeneration of the photoreceptor cell body. The *dOPA1* knockdown caused a significant decrease in
175 the number of rhabdomeres per ommatidium in 1-week-old adults (Figure 3G–J, quantification in 3K).
176 Interestingly, although the retinal axons had already decreased on the day of eclosion, the ommatidia
177 remained intact (Figure 3F and 3K). Note that the ommatidia in R7 remained intact after one week
178 (Figure 3J). Our results indicate that the *dOPA1* knockdown causes degeneration in both axonal
179 terminals and cell bodies, with the neuronal degeneration starting from the axons and continuing in
180 the cell bodies. This suggests that cell body loss precedes neurite retrograde degeneration, as described
181 in many neurodegenerative diseases (Wang et al., 2012).

182 To test whether our RNAi results reflect *dOPA1* downregulation, we performed mutant
183 analysis of the *dOPA1* gene in retinal axons. For this, we used the $dOPA1^{s3475}$ hypomorphic mutant
184 allele, which has a P-element insertion in exon 2 (Yarosh et al., 2008). Somatic mosaic clones were
185 generated in the retinal axons using the FLP/FRT system (Golic and Lindquist, 1989) because
186 homozygous mutant alleles are embryonic lethal (Sandoval et al., 2014; Yarosh et al., 2008). Using
187 MeDUsA, we found a significantly lower number of *dOPA1* mutant retinal axons than in controls one
188 day after eclosion (Figure 4A and B, quantification in 4D). To determine if *dOPA1* is responsible for
189 axon neurodegeneration, we observed the *dOPA1* mutant axons by expressing full-length versions of

190 *dOPA1* in the photoreceptors at one day after eclosion and found that dOPA1 expression significantly
191 rescued the axonal degeneration (Figure 4C, quantification in Figure 4D). Our results indicate that
192 *dOPA1* is necessary for maintaining the number of retinal axons in the *Drosophila* visual system. In
193 conclusion, the neurodegeneration observed in the LOF of *dOPA1* is due to the progressive loss of
194 retinal axons, as well as the mammal optic nerve.

195

196 **Investigating disease mutations in OPA1 using a fly DOA model to confirm their pathological**
197 **significance**

198 Our observations in *dOPA1* LOF flies confirmed mitochondria fragmentation, increased ROS levels,
199 and degeneration of retinal axons, as reported in mammals. These data indicated that the function of
200 *OPA1* may be conserved across *Drosophila* and humans. Thus, we tested whether *hOPA1* could
201 effectively replace *dOPA1* in flies by generating a transgenic organism to express *hOPA1* in
202 *Drosophila*. Following the UAS sequence, that the yeast-derived transcription factor Gal4 binds, the
203 construct included an HA tag, followed by the *hOPA1* gene, and a myc tag (Figure 5A). This construct
204 was expressed in *Drosophila* and protein expression was confirmed by Western blotting. The HA tag,
205 attached to the N-terminus, was immunoblotted resulting in a band of the expected full-length size

206 (Figure 5B). For the myc tag at the C-terminus, a strong band and two weak bands were observed at
207 the upper and lower positions (Figure 5B).

208 Using this UAS-hOpa1, we performed rescue experiments. *hOPA1* expression in the retinal
209 axons of the *dOPA1* mutant, which generated somatic cell clones, significantly rescued the number of
210 axons (Figure 5C). These results suggest that *hOPA1* and *dOPA1* are interchangeable. We also
211 generated and expressed the *hOPA1* mutation 2708_2711del, which is known to cause DOA, the
212 I382M mutation, located in the GTPase domain and associated with DOA, as well as the D438V and
213 R445H mutations, also located in the GTPase domain and associated with DOA plus. The 2708-
214 2711del mutation was weakly detectable by HA but not detectable by myc due to the frameshift caused
215 by the deletion (Fig. 5B). This appears to be a result from the mutation to generate a truncated protein,
216 as previously reported (Zanna et al., 2008). The I382M, D438V, and R445H mutations had similar
217 expression levels to the WT *hOPA1* (Figure 5B). However, the expression of these mutations in retinal
218 axons failed to rescue the *dOPA1* deficiency to the same extent as the WT *hOPA1* (Figure 5C). These
219 results suggest that these mutations result in functional impairment, consistent with the established
220 understanding (Zanna et al., 2008). Importantly, unlike the D438V and R445H mutations, the 2708-
221 2711del and I382M mutations could be weakly rescued. This suggests that these mutations result in
222 LOF, but may retain some residual activity. This is consistent with the characterization of I382M as a
223 hypomorph (Del Dotto et al., 2018). These findings are also in line with the observed severity of the

224 associated diseases, DOA and DOA plus. As the D438V and R445H mutations were not significantly
225 rescued, unlike the 2708-2711del and I382M mutations. Our results demonstrate that our model can
226 quantitatively measure the degree of LOF.

227

228 **Distinction between LOF and DN mutations in *hOPA1* linked to DOA or DOA plus**

229 Currently, the *hOPA1* mutations that contribute to DOA plus have been primarily located in the
230 GTPase domain of *hOPA1*. The role of *hOPA1* as a GTPase is facilitated by its ability to form a
231 polymer via the GED domain and Middle domain (Li et al., 2019). This led to the hypothesis that
232 mutations in the GTPase domain can interact with WT hOPA1 but cannot activate the GTPase activity
233 to show a DN effect. However, it has been challenging to clarify whether these mutations are DN or
234 LOF, as there is a significant number of LOF mutations in the GTPase domain. Given that *dOPA1* can
235 be substituted with *hOPA1*, we suspected that a DN effect could also be achieved by expressing the
236 D438V or R445H mutations in the WT background. However, the axons did not degenerate despite
237 expression and monitoring for two weeks in adult flies (Fig. 6A). The amino acid sequences of hOPA1
238 and dOPA1 are highly conserved (72% identity), particularly in the GTPase domain. The Middle and
239 GED domains are also relatively well-preserved, with 54% and 64% agreement, respectively (Figure
240 S2). These results imply that, although *dOPA1* and *hOPA1* are functionally interchangeable, they may

241 not interact with each other. Consequently, we expressed *hOPA1* in the photoreceptor depleted of
242 *dOPA1* by somatic clone; under these conditions, we further expressed *hOPA1* WT, 2708-2711del,
243 and mutations in the GTPase domains, including R445H, I382M, and D438V. This allowed *hOPA1*
244 to interact with itself and to verify the DN effect. As a result, the expression of the WT, 2708del, and
245 I382M did not result in any changes when rescued by *hOPA1* substitution (Figure 6B). However, the
246 rescue was significantly suppressed for D438V and R445H, which are known to cause DN; thus, the
247 DN effect could be replicated (Figure 6B). In conclusion, we established an experimental model that
248 can separate LOF and DN, the pathological significance of *hOPA1* mutations.

249

250 **Discussion**

251 In this study, we found that LOF of *dOPA1* in *Drosophila* can imitate human DOA, in which the optic
252 nerve degenerates. We were successful in reversing this degeneration by expressing *hOPA1* (Figure
253 6C). However, we could not rescue any previously reported mutations known to cause either DOA or
254 DOA plus. In the context of rescuing the retinal axons of the *dOPA1* mutant by expressing the WT of
255 *hOPA1*, it was observed that only the DOA plus mutations suppressed the rescue (Figure 6C). This
256 allowed us to distinguish between LOF and DN mutations in *hOPA1*. The fly model developed in this
257 study will allow investigating new *hOPA1* mutations for DOA or DOA plus.

258 Our established fly model is the first simple organism allowing observation of degeneration
259 of axons in the optic nerve and fragmentation of mitochondria. Previously, the function of *OPA1* in
260 mice (*mOPA1*) was substituted by *hOPA1* (Del Dotto et al., 2017; Sarzi et al., 2018). Here we
261 demonstrated that the function of *dOPA1* can also be substituted by *hOPA1*. Thus, the function of
262 *OPA1* is conserved across a wide range of species but our fly model has the advantage of allowing
263 rapid observation of phenotypes. In the mouse model of DOA with the heterozygous deletion of the
264 *mOPA1* gene at positions 329–355 (Alavi et al., 2007) or delTTAG mutant (Sarzi et al., 2012), a
265 decrease in the number of RGC was observed after 17 months or 16 months of age, respectively. To
266 save time, using a fly model for quick analysis and direct observation of retinal axons would be useful.
267 Previous models using nematodes, flies, and zebrafish did not observe axonal degeneration directly,
268 but our new model has made this possible. As a result, our model has the potential to be used for
269 screening for modifiers of unclear molecular pathologies and drug screening.

270 Our model could also demonstrate the pathological significance of *hOPA1* mutations and be
271 used for genetic diagnosis to differentiate between LOF and DN mutations. Our results for LOF or
272 DN segmentation were consistent with previously reported yeast models (Del Dotto et al., 2018) and
273 fibroblasts obtained from patients with OPA1 mutations (Kane et al., 2017), and confirmed the
274 conserved function of *OPA1* across species. A major advantage of the *Drosophila* model over yeast
275 or fibroblasts, is that we can observe a phenotype that mimics the actual disease state of axonal

degeneration in retinal axons and analyze it not only at the molecular level, but also the structural level of axons and mitochondria. The transgenic *Drosophila* of disease-associated *hOpa1* mutations created in this study can also serve to understand the pathophysiology of these mutations.

Advances in genome analysis allowed the identification of many variants and genetic mutations associated with DOA using next-generation sequencing. This could confirm diagnoses and identify new forms of DOA. The widespread use of these sequencers has also created new challenges, such as the growing number of variants of unknown significance (VUS) in publicly available databases such as CliniVar for DOA. These variants are categorized as pathogenic, likely pathogenic, VUS, likely benign, or benign, and the number of VUS is increasing as more variants are registered. The ClinVar database had classified 110 out of 319 *Opa1* variants as VUS at the end of 2019. By the end of 2022, this number had increased to 357 out of 840, indicating an increase from 34% to 42% over the last three years (Henrie et al., 2018). This trend suggests that the number of VUS in *Opa1* may continue to increase in the future. Analyzing VUS requires testing the effects of a mutation *in vitro* or *in vivo*; this can be expensive and time-consuming without prior confirmation or high probability of pathological significance. However, our fly model can be used to easily and inexpensively determine the pathological effects of disease-causing gene mutations among the growing number of rare mutations identified in DOA.

293 In this study, we tested the effect of expressing the D438V and R445H mutations in the
294 *dOPA1* background and found that retinal axons did not degenerate. Regarding the interactions among
295 OPA1 proteins, in yeast Mgm1, K854 in the region near the C-terminus is important for aggregation,
296 and it becomes an oligomer to increase the activity of GTPase (Rujiviphat et al., 2009). Although
297 hOPA1 normally has low GTPase activity, its interaction with negatively charged phospholipids such
298 as cardiolipin causes hOPA1 to aggregate, increasing GTP hydrolysis activity (Ban et al., 2010). In
299 the thermophilic fungus *Chaetomium thermophilum*, Mgm1 forms a dimer and then a tetramer at the
300 C-terminal Stalk domain of Mgm1 (Faelber et al., 2019). Structural analysis also predicted that the
301 Middle and GED domains are necessary for dimer and oligomer formation in hOPA1 (Li et al., 2019).
302 In addition, peptide-binding assays have revealed that the coiled-coil domain, which is part of the
303 GED domain, is required for hOPA1 interactions (Akepati et al., 2008). Comparing the amino acid
304 sequences of hOPA1 and dOPA1, the Middle and GED domains, which are necessary for interactions
305 between OPA1 molecules, exhibit concordance rates of 54.3% and 63.6%, respectively. These
306 percentages are low compared to the 71.8% identity observed in the GTPase domains. These suggest
307 that the OPA1 homologs of each species form oligomers with their unique OPA1. Note that the
308 expression of $dOPA1^{K273A}$, a presumably GTPase-negative form of *dOPA1* (Tsuyama et al., 2017),
309 degenerated retinal axons (data not shown). These results imply that, while dOPA1 and hOPA1 are
310 interchangeable, they may not interact with each other. This could pave the way for the development

311 of a chimeric hOPA1, which would retain its functional properties while avoiding the interaction with
312 endogenous hOPA1. Such chimeric hOPA1 could potentially be used as gene therapy since induced
313 pluripotent stem cells have been generated from a patient with R445H (Sladen et al., 2021).

314 OPA1 has been implicated in various other diseases as well, including normal tension
315 glaucoma (Powell et al., 2003; Yu-Wai-Man et al., 2010b), multiple sclerosis (Verny et al., 2008; Yu-
316 Wai-Man et al., 2016), Parkinson's disease and dementia (Carelli et al., 2015; Lynch et al., 2017), and
317 cardiomyopathy (Spiegel et al., 2016). Although the connection between these diseases and OPA1 is
318 not fully understood, further research on DOA may provide a deeper insight into this relationship. In
319 the future, pathological analysis using the present model could have implications for understanding
320 the mechanisms underlying these diseases.

321 DOA has also been reported to involve mitochondrial DNA (mtDNA) depletion (Amati-
322 Bonneau et al., 2008), but our model, while useful for nuclear gene analysis, is limited for mtDNA
323 analysis. The gene content in the *Drosophila* mtDNA genome is similar as that in vertebrates, but the
324 gene order and distribution on both DNA strands differ. mOPA1 interacts with mtDNA nucleoids
325 through exon 4b binding to mtDNA D-loops, independent of mitochondrial fusion (Yang et al., 2020).
326 However, the homologous region of mOPA1 or hOPA1 to exon4b is not found in *Drosophila*, and the
327 D-loop of mtDNA has not been found in cultured cells of flies or in mtDNA of embryos using electron

328 microscopy (Rubenstein et al., 1977). In addition, while the D-loop is involved in mtDNA replication
329 in humans (Fish et al., 2004), the A + T region is the origin of replication in mtDNA replication in
330 *Drosophila* (Goddard and Wolstenholme, 1978). Thus, there may be differences in the mechanism of
331 mtDNA replication between humans and flies (Garesse and Kaguni, 2005). Therefore, the association
332 of dOPA1 with mtDNA may differ from that in mammals and the regulatory mechanism of mtDNA
333 homeostasis in which dOPA1 is involved requires further investigation.

334 Another limitation of our model is that the molecular mechanisms underlying the formation
335 of long-form OPA1 (L-OPA1) and short-form OPA1 (S-OPA1), which are well analyzed in mammals
336 (MacVicar and Langer, 2016), have not been elucidated in *Drosophila*. In hOPA1, S1 or S2 sites are
337 processed by the i-AAA protease OMA1 and Yme1L respectively to produce S-hOPA1 (Anand et al.,
338 2014). Despite the fact that Yme1L is conserved in *Drosophila*, it has been involved in the degradation
339 of the dOPA1 protein rather than its cleavage by dYme1L (Liu et al., 2020). Moreover, the cleavage
340 site for i-AAA does not exist in dOPA1 (Olichon et al., 2007). Regarding other proteases, yeast Mgm1
341 is processed by the rhomboid protease Pcp1 (Esser et al., 2002; Herlan et al., 2003). However, the
342 Rhomboid-7, a Pcp1 ortholog of *Drosophila*, was not required for dOPA1 processing (Whitworth et
343 al., 2008). Although hOPA1 expression in *Drosophila* has identified three different sizes of hOPA1
344 in our Western blotting result, it is unclear how they are cleaved. The upper band was expected as the
345 full-length hOPA1 including the mitochondria import sequence (MIS). Since the Middle and the

346 lowest bands were not present in HA-tagged samples, it is possible that the bands at the Middle size
347 represent the long-form hOPA1 (L-hOPA1) in which probably MIS was processed. The band detected
348 at the lowest position may represent a short form of hOPA1 (S-hOPA1). However, *Drosophila* does
349 not have OMA1, an i-AAA protease that cleaves the S1 site. Although another i-AAA protease that
350 cleaves the S2 site, YME1L, is conserved, our expressed hOPA1 is isoform 1 and lacks the S2 site
351 (Fig. 5a). Therefore, it is not clear how S-hOPA1 is processed in *Drosophila*. The anti-dOPA1
352 antiserum detects three bands in the overexpression of a FLAG-tagged dOPA1 construct (Poole et al.,
353 2010), suggesting a molecular mechanism by which dOPA1, like yeast and mammals, is cleaved after
354 translation. However, the proteases involved in the mechanism are not yet clarified. Whether
355 *Drosophila's* endogenous mechanisms can be used to study how L-OPA1 and S-OPA1 are involved
356 in DOA remains unclear.

357 In this study, we established a new model of DOA in *Drosophila*, in which we discovered
358 the following: 1. We could replicate the human disease of optic nerve degeneration, allowing rapid
359 genetic disease analysis. 2. We could distinguish the LOF and DN effects of *hOPA1*. These findings
360 can reveal the pathological significance of *de novo* mutations and are useful in diagnosing DOA or
361 DOA plus. Additionally, while *hOPA1* is the major gene involved in DOA, other genes involved in
362 DOA and interacting proteins have not been investigated yet. Our model can be used for pathological

363 modifier screening, exploring modifiers, and contributing to drug development. In the future, we hope

364 to provide insights that can be applied to the fundamental treatment of DOA.

365

366 **Materials and Methods**

367 ***Fly strains***

368 Flies were maintained at a temperature of 25°C on standard fly food. For the knockdown experiments

369 (Figure 1C–E, 1F–H, 2A–C, 3B–K), flies were maintained at 29°C. Female flies were used in all

370 experiments to ensure consistency in the number of retinal axons. The following fly strains were

371 obtained from the Bloomington Drosophila Stock Center: *GMR-Gal4* (#1104), *UAS-dicer2(III)*

372 (#24651), *UAS-mito-HA-GFP* (#8443), *UAS-mCherry-mito* (#66532), *UAS-dOPA1 RNAi* (#32358),

373 *UAS-Milton RNAi* (#44477), *FRT42D, GMR-hid, l(2)cl-R11[1]/CyO; ey-Gal4, UAS-flp* (#5251), *ey-*

374 *FLP; FRT42D, l(2)cl-R11[1]/CyO* (#5617), and *Tub-Gal80*^{TS} (#7017). The *40D-UAS* (VDRC 60101)

375 fly strain was obtained from the Vienna Drosophila Resource Center. *FRT19* (Kyoto 101231),

376 *FRT42D* (Kyoto 101878), and *dOPA1*^{s3475} (Kyoto 111438) were obtained from the Kyoto Drosophila

377 Stock Center. The *UAS-dOPA1-HA* was generously provided by T. Uemura (Kyoto University, Japan).

378

379 ***Generation of transgenic flies***

380 The cDNA for WT, I382M, D438V, R445H, and 2708-2711del forms of *hOPA1* [NM_015560.3] were
381 generated by Vectorbuilder Inc. (Yokohama, Japan). Then, the HA-hOPA1-myc sequence was
382 amplified and inserted into pJFRC81-10XUAS-IVS-Syn21-GFP-p10 (ID36432, Addgene,
383 Massachusetts, USA) using primers with the N-terminal containing the Kozak and HA sequences
384 (TTACTTCAGGCGGCCGCGGCCAAAATGTACCCATACGATGTTCCAGATTAC) and the C-
385 terminal containing the myc sequence
386 (TTAAAAACGATTCATTCTAGTTACAGATCCTCTTCTGAGATGAGTTTTTGTTCTTTCTCCT
387 GATGAAGAGCTTCAATG). To confirm production of the complete coding sequence, it was
388 bidirectionally sequenced using the Sanger method. These plasmids were injected into embryos and
389 integrated into the aTTP2 landing site (WellGenetics, Taipei, Taiwan).
390

391 ***Immunohistochemistry and imaging***

392 Immunohistochemistry was performed as described previously (Sugie et al., 2017). The following
393 antibodies were used: rat anti-HA (3F10, 1:400; Roche, Switzer land), mouse anti-Chaoptin (24B10,
394 1:25; Developmental Studies Hybridoma Bank, USA), rat anti-CadN (DN-Ex#8, 1:50; Developmental
395 Studies Hybridoma Bank), anti-rat Alexa Fluor 488 (1:400; Thermo Fisher Scientific, USA), anti-
396 mouse Alexa Fluor 488 (1:400; Thermo Fisher Scientific), anti-mouse Alexa Fluor 568 (1:400;

397 Thermo Fisher Scientific), and anti-rat Alexa Fluor 633 (1:400; Thermo Fisher Scientific). Specimens
398 were mounted using a Vectashield mounting medium (Vector Laboratories, USA). Images were
399 captured using an FV3000 confocal microscope (Olympus, Japan) or a C2 (Nikon, Japan) confocal
400 microscope for Figure S1 and processed using the IMARIS software (Oxford Instruments, UK) or Fiji
401 software, an open-source image analysis software (Schindelin et al., 2012).

402

403 ***Electron microscopy***

404 Fly heads were fixed overnight with 2.5% glutaraldehyde and 2% paraformaldehyde in 0.1 M sodium
405 cacodylate buffer. Heads were then post-fixed with 1% osmium tetroxide, dehydrated in ethanol, and
406 embedded in Epon. Ultra-thin tangential sections of the laminas (70 nm) were stained with uranyl
407 acetate and lead citrate. Random retinas or lamina sections were imaged at a magnification of ×100 k
408 with a VELETA CCD Camera (Olympus Soft Imaging Solutions) mounted on a JEM 1010
409 transmission electron microscope (JEOL). The area corresponding to the mitochondria in the R1–6
410 axons of the lamina was measured using the freehand line tool in NIS elements (Nikon).

411

412 ***Quantification of mito-GFP intensity in retinal axons and retina***

413 To measure the relative intensity of mito-GFP in the photoreceptor R7/8 axons of the medulla, the

414 imaging analysis software IMARIS was used. First, the M1–6 layers of the medulla, including the
415 R7/8 axons, were manually covered using the surface function. Then, the surface area was masked,
416 the surface of the left axons was stained with anti-Chaoptin, and the mito-GFP signal was generated
417 automatically using the surface function. Finally, the voxel number of the mito-GFP surface was
418 divided by the voxel number of the R axon surface. These quantifications were performed by
419 experimenters blind to the genotype.
420
421 ***Mitochondrial superoxide detection and quantification***
422 The ROS level was determined using the MitoSox Red Mitochondrial Superoxide Indicator
423 (Invitrogen). The procedure involved dissecting adult brains in phosphate-buffered saline (PBS),
424 transferring them to 5 μM MitoSox solution, and incubating them for 10 min in the dark at room
425 temperature. The brains were then washed with PBS containing 20% Vectashield (Vector Laboratories),
426 followed by sequential washes with PBS containing 40% and 60% Vectashield. The samples were
427 mounted in Vectashield and scanned using an FV3000 confocal microscope (Olympus). To quantify
428 the ROS level in photoreceptor R7/8 axons, the IMARIS software (Bitplane) was used for imaging
429 analysis. The software generated automatic surfaces of the MitoSox and mito-GFP signals. Then, the
430 ROS level was calculated by dividing the voxel number of the MitoSox surface on the mito-GFP
431 surface by the voxel number of the mito-GFP surface. These quantifications were performed by

432 experimenters blind to the genotype.

433

434 ***Western blot analysis of the whole Drosophila body***

435 Protein expression was temporarily controlled in the whole body by combining *Tub-Gal4* and *Tub-*
436 *GAL80^{TS}*. The flies crossed with each hOPA1 variant were raised at a permissive temperature (20°C),
437 and newly eclosed females were held at the restrictive temperature (29°C). After two days, 10 whole
438 bodies were sonicated (2 x 30 s) using a Q55 sonicator (Qsonica, Newtown, CT, USA) in lysis buffer
439 (10 mM Tris–HCl, pH 7.5, 150 mM NaCl, 1 mM EDTA, 2% DDM) supplemented with 1:1000 (v/v)
440 Protease Inhibitor Cocktail Set III (Calbiochem, La Jolla, CA, USA). Rat anti-HA (3F10, 1:5000;
441 Roche, Mannheim, Germany), mouse anti-myc (9B11, 1: 10000; Cell Signaling Technology, Danvers,
442 MA, USA), and mouse anti-α-Tubulin (T9026, 1:100,000; Sigma‐Aldrich, St. Louis, MO, USA)
443 antibodies were used for Western blotting.

444

445 ***Pairwise alignment of hOPA1 and dOPA1***

446 The amino acid sequences for hOPA1 and dOPA1 were referenced from NM_015560.3 and
447 NM_166040.2, respectively, and aligned using the EMBOSS Needle. The GTPase, Middle, and GED
448 domains in dOPA1 were identified by cross-referencing the previously described amino acid positions

449 of these domains in hOPA1 (Liesa et al., 2009). The degree of identity between the aligned amino acid

450 sequences was subsequently determined.

451

452 ***Experimental design and statistical analyses***

453 Experimental analyses were performed using Prism 9 (GraphPad Software, San Diego, CA, USA).

454 For Figures 3–5, data were analyzed using t tests (and nonparametric tests) and Mann-Whitney tests.

455 For Figures 1, 2, 6, and 7, differences among multiple groups were examined using the Kruskal−Wallis

456 test followed by the two-stage linear step-up procedure of Benjamini, Krieger, and Yekutieli tests. The

457 null hypothesis was rejected at a 0.05 level of significance. Sample sizes are indicated in each figure.

458 The number of retinal axons and rhabdomeres, the intensity of mito-GFP and MitoSox, the

459 mitochondrial area and the classification, and the corrected *P* values are described in the Results

460 section. All data are expressed as the mean ± SEM.

461

462 ***Acknowledgements***

463 We would like to thank Dr Uemura for providing us with the transgenic fly strain. The Ministry of

464 Education, Culture, Sports, Science, and Technology of Japan (#18K14835, #18J00367 and

465 #21K15619 to Y.N., #21K06184 to S.H.S., #16H06457, #21H02483 and 21H05682 to T.S.,

466 #17H04983, #19K22592 and #21H02837 to A.S.), the Japan Agency for Medical Research and
467 Development (AMED) (#JP22ek019484s) to A.S., NIG–JOINT to E.S., Takeda Science Foundation
468 Takeda Visionary Research Grant to T.S., Takeda Science Foundation Life Science Research Grant to
469 A.S., and GSK Japan Research Grant 2022 [AS2021A000166849] to A.S..

470

471 ***References***

472 Akepati VR, Müller EC, Otto A, Strauss HM, Portwich M, Alexander C. 2008. Characterization of OPA1
473 isoforms isolated from mouse tissues. *J Neurochem* **106**:372–383. doi:10.1111/j.1471-
474 4159.2008.05401.x

475 Alavi M V., Bette S, Schimpf S, Schuettauf F, Schraermeyer U, Wehrl HF, Ruttiger L, Beck SC, Tonagel
476 F, Pichler BJ, Knipper M, Peters T, Laufs J, Wissinger B. 2007. A splice site mutation in the
477 murine Opa1 gene features pathology of autosomal dominant optic atrophy. *Brain* **130**:1029–1042.
478 doi:10.1093/brain/awm005

479 Alexander C, Votruba M, Pesch UEA, Thiselton DL, Mayer S, Moore A, Rodriguez M, Kellner U, Leo-
480 Kottler B, Auburger G, Bhattacharya SS, Wissinger B. 2000. OPA1, encoding a dynamin-related
481 GTPase, is mutated in autosomal dominant optic atrophy linked to chromosome 3q28. *Nat Genet*
482 **26**:211–215. doi:10.1038/79944

483 Amati-Bonneau P, Odent S, Derrien C, Pasquier L, Malthiéry Y, Reynier P, Bonneau D. 2003. The

484 association of autosomal dominant optic atrophy and moderate deafness may be due to the R445H
485 mutation in the OPA1 gene. *Am J Ophthalmol* **136**:1170–1171. doi:10.1016/S0002-9394(03)00665-
486 2
487 Amati-Bonneau P, Valentino ML, Reynier P, Gallardo ME, Bornstein B, Boissière A, Campos Y, Rivera
488 H, De La Aleja JG, Carroccia R, Iommarini L, Labauge P, Figarella-Branger D, Marcorelles P,
489 Furby A, Beauvais K, Letournel F, Liguori R, La Morgia C, Montagna P, Liguori M, Zanna C,
490 Rugolo M, Cossarizza A, Wissinger B, Verny C, Schwarzenbacher R, Martín MÁ, Arenas J, Ayuso
491 C, Garesse R, Lenaers G, Bonneau D, Carelli V. 2008. OPA1 mutations induce mitochondrial DNA
492 instability and optic atrophy "plus" phenotypes. *Brain* **131**:338–351. doi:10.1093/brain/awm298
493 Anand R, Wai T, Baker MJ, Kladt N, Schauss AC, Rugarli E, Langer T. 2014. The i-AAA protease
494 YME1L and OMA1 cleave OPA1 to balance mitochondrial fusion and fission. *J Cell Biol* **204**:919–
495 929. doi:10.1083/jcb.201308006
496 Ban T, Heymann JAW, Song Z, Hinshaw JE, Chan DC. 2010. OPA1 disease alleles causing dominant
497 optic atrophy have defects in cardiolipin-stimulated GTP hydrolysis and membrane tubulation.
498 *Hum Mol Genet* **19**:2113–2122. doi:10.1093/hmg/ddq088
499 Brand AH, Perrimon N. 1993. Targeted gene expression as a means of altering cell fates and generating
500 dominant phenotypes. *Development* **118**:401–415. doi:10.1242/dev.118.2.401
501 Byrne JJ, Soh MS, Chandhok G, Vijayaraghavan T, Teoh JS, Crawford S, Cobham AE, Yapa NMB,

502 Mirth CK, Neumann B. 2019. Disruption of mitochondrial dynamics affects behaviour and lifespan
503 in Caenorhabditis elegans. *Cell Mol Life Sci* **76**:1967–1985. doi:10.1007/s00018-019-03024-5
504 Carelli V, Musumeci O, Caporali L, Zanna C, La Morgia C, Del Dotto V, Porcelli AM, Rugolo M,
505 Valentino ML, Iommarini L, Maresca A, Barboni P, Carbonelli M, Trombetta C, Valente EM,
506 Patergnani S, Giorgi C, Pinton P, Rizzo G, Tonon C, Lodi R, Avoni P, Liguori R, Baruzzi A,
507 Toscano A, Zeviani M. 2015. Syndromic parkinsonism and dementia associated with OPA1
508 missense mutations. *Ann Neurol* **78**:21–38. doi:10.1002/ana.24410
509 Davies VJ, Hollins AJ, Piechota MJ, Yip W, Davies JR, White KE, Nicols PP, Boulton ME, Votruba M.
510 2007. Opa1 deficiency in a mouse model of autosomal dominant optic atrophy impairs
511 mitochondrial morphology, optic nerve structure and visual function. *Hum Mol Genet* **16**:1307–
512 1318. doi:10.1093/hmg/ddm079
513 Del Dotto V, Carelli V. 2021. Dominant Optic Atrophy (DOA): Modeling the Kaleidoscopic Roles of
514 OPA1 in Mitochondrial Homeostasis. *Front Neurol*. doi:10.3389/fneur.2021.681326
515 Del Dotto V, Fogazza M, Musiani F, Maresca A, Aleo SJ, Caporali L, La Morgia C, Nolli C, Lodi T,
516 Goffrini P, Chan D, Carelli V, Rugolo M, Baruffini E, Zanna C. 2018. Deciphering OPA1
517 mutations pathogenicity by combined analysis of human, mouse and yeast cell models. *Biochim*
518 *Biophys Acta - Mol Basis Dis* **1864**:3496–3514. doi:10.1016/j.bbadis.2018.08.004
519 Del Dotto V, Mishra P, Vidoni S, Fogazza M, Maresca A, Caporali L, McCaffery JM, Cappelletti M,

520 Baruffini E, Lenaers G, Chan D, Rugolo M, Carelli V, Zanna C. 2017. OPA1 Isoforms in the
521 Hierarchical Organization of Mitochondrial Functions. *Cell Rep* **19**:2557–2571.
522 doi:10.1016/j.celrep.2017.05.073
523 Delettre C, Lenaers G, Griffoin JM, Gigarel N, Lorenzo C, Belenguer P, Pelloquin L, Grosgeorge J, Turc-
524 Carel C, Perret E, Astarie-Dequeker C, Lasquellec L, Arnaud B, Ducommun B, Kaplan J, Hamel
525 CP. 2000. Nuclear gene OPA1, encoding a mitochondrial dynamin-related protein, is mutated in
526 dominant optic atrophy. *Nat Genet* **26**:207–210. doi:10.1038/79936
527 Deng H, Dodson MW, Huang H, Guo M. 2008. The Parkinson's disease genes pink1 and parkin promote
528 mitochondrial fission and/or inhibit fusion in Drosophila. *Proc Natl Acad Sci U S A* **105**:14503–
529 14508. doi:10.1073/pnas.0803998105
530 Eijkenboom I, Vanoevelen JM, Hoeijmakers JGJ, Wijnen I, Gerards M, Faber CG, Smeets HJM. 2019. A
531 zebrafish model to study small-fiber neuropathy reveals a potential role for GDAP1. *Mitochondrion*
532 **47**:273–281. doi:10.1016/j.mito.2019.01.002
533 Esser K, Tursun B, Ingenhoven M, Michaelis G, Pratje E. 2002. A novel two-step mechanism for
534 removal of a mitochondrial signal sequence involves the mAAA complex and the putative
535 rhomboid protease Pcp1. *J Mol Biol* **323**:835–843. doi:10.1016/S0022-2836(02)01000-8
536 Faelber K, Dietrich L, Noel JK, Wollweber F, Pfitzner AK, Mühleip A, Sánchez R, Kudryashev M,
537 Chiaruttini N, Lilie H, Schlegel J, Rosenbaum E, Hessenberger M, Matthaeus C, Kunz S, von der

538 Malsburg A, Noé F, Roux A, van der Laan M, Kühlbrandt W, Daumke O. 2019. Structure and
539 assembly of the mitochondrial membrane remodelling GTPase Mgm1. *Nature* **571**:429–433.
540 doi:10.1038/s41586-019-1372-3
541 Ferré M, Caignard A, Milea D, Leruez S, Cassereau J, Chevrollier A, Amati-Bonneau P, Verny C,
542 Bonneau D, Procaccio V, Reynier P. 2015. Improved locus-specific database for OPA1 mutations
543 allows inclusion of advanced clinical data. *Hum Mutat* **36**:20–25. doi:10.1002/humu.22703
544 Fish J, Raule N, Attardi G. 2004. Discovery of a major D-loop replication origin reveals two modes of
545 human mtDNA synthesis. *Science (80-)* **306**:2098–2101. doi:10.1126/science.1102077
546 Frezza C, Cipolat S, Martins de Brito O, Micaroni M, Beznoussenko G V., Rudka T, Bartoli D, Polishuck
547 RS, Danial NN, De Strooper B, Scorrano L. 2006. OPA1 Controls Apoptotic Cristae Remodeling
548 Independently from Mitochondrial Fusion. *Cell* **126**:177–189. doi:10.1016/j.cell.2006.06.025
549 Garesse R, Kaguni LS. 2005. A Drosophila model of mitochondrial DNA replication: Proteins, genes and
550 regulation. *IUBMB Life*. doi:10.1080/15216540500215572
551 Goddard JM, Wolstenholme DR. 1978. Origin and direction of replication in mitochondrial DNA
552 molecules from Drosophila melanogaster. *Proc Natl Acad Sci U S A* **75**:3886–3890.
553 doi:10.1073/pnas.75.8.3886
554 Golic KG, Lindquist S. 1989. The FLP recombinase of yeast catalyzes site-specific recombination in the
555 drosophila genome. *Cell* **59**:499–509. doi:10.1016/0092-8674(89)90033-0

556 Henrie A, Hemphill SE, Ruiz-Schultz N, Cushman B, DiStefano MT, Azzariti D, Harrison SM, Rehm
557 HL, Eilbeck K. 2018. ClinVar Miner: Demonstrating utility of a Web-based tool for viewing and
558 filtering ClinVar data. *Hum Mutat* **39**:1051–1060. doi:10.1002/humu.23555
559 Herlan M, Vogel F, Bornhövd C, Neupert W, Reichert AS. 2003. Processing of Mgm1 by the rhomboid-
560 type protease Pcp1 is required for maintenance of mitochondrial morphology and of mitochondrial
561 DNA. *J Biol Chem* **278**:27781–27788. doi:10.1074/jbc.M211311200
562 Kanazawa T, Zappaterra MD, Hasegawa A, Wright AP, Newman-Smith ED, Buttle KF, McDonald K,
563 Mannella CA, Van Der Bliek AM. 2008. The C. elegans Opa1 homologue EAT-3 is essential for
564 resistance to free radicals. *PLoS Genet* **4**. doi:10.1371/journal.pgen.1000022
565 Kane MS, Alban J, Desquiret-Dumas V, Gueguen N, Ishak L, Ferre M, Amati-Bonneau P, Procaccio V,
566 Bonneau D, Lenaers G, Reynier P, Chevrollier A. 2017. Autophagy controls the pathogenicity of
567 OPA1 mutations in dominant optic atrophy. *J Cell Mol Med* **21**:2284–2297.
568 doi:10.1111/jcmm.13149
569 Lenaers G, Neutzner A, Le Dantec Y, Jüschke C, Xiao T, Decembrini S, Swirski S, Kieninger S, Agca C,
570 Kim US, Reynier P, Yu-Wai-Man P, Neidhardt J, Wissinger B. 2021. Dominant optic atrophy:
571 Culprit mitochondria in the optic nerve. *Prog Retin Eye Res*. doi:10.1016/j.preteyeres.2020.100935
572 Li D, Wang J, Jin Z, Zhang Z. 2019. Structural and evolutionary characteristics of dynamin-related
573 GTPase OPA1. *PeerJ* **2019**. doi:10.7717/peerj.7285

574 Liesa M, Palacín M, Zorzano A. 2009. Mitochondrial dynamics in mammalian health and disease.
575 *Physiol Rev*. doi:10.1152/physrev.00030.2008
576 Liu W, Duan X, Xu L, Shang W, Zhao J, Wang L, Li JC, Chen CH, Liu JP, Tong C. 2020. Chchd2
577 regulates mitochondrial morphology by modulating the levels of Opa1. *Cell Death Differ* **27**:2014–
578 2029. doi:10.1038/s41418-019-0482-7
579 Lynch DS, Loh SHY, Harley J, Noyce AJ, Martins LM, Wood NW, Houlden H, Plun-Favreau H. 2017.
580 Clinical/Scientific Notes: Nonsyndromic Parkinson disease in a family with autosomal dominant
581 optic atrophy due to opa1 mutations. *Neurol Genet* **3**. doi:10.1212/NXG.0000000000000188
582 MacVicar T, Langer T. 2016. OPA1 processing in cell death and disease - the long and short of it. *J Cell*
583 *Sci*. doi:10.1242/jcs.159186
584 McQuibban GA, Lee JR, Zheng L, Juusola M, Freeman M. 2006. Normal Mitochondrial Dynamics
585 Requires Rhomboid-7 and Affects Drosophila Lifespan and Neuronal Function. *Curr Biol* **16**:982–
586 989. doi:10.1016/j.cub.2006.03.062
587 Meglei G, McQuibban GA. 2009. The dynamin-related protein Mgm1p assembles into oligomers and
588 hydrolyzes GTP to function in mitochondrial membrane fusion. *Biochemistry* **48**:1774–1784.
589 doi:10.1021/bi801723d
590 Newsome TP, Åsling B, Dickson BJ. 2000a. Analysis of Drosophila photoreceptor axon guidance in eye-
591 specific mosaics. *Development* **127**:851–860. doi:10.1242/dev.127.4.851

592 Newsome TP, Schmidt S, Dietzl G, Keleman K, Åsling B, Debant A, Dickson BJ. 2000b. Trio combines
593 with dock to regulate Pak activity during photoreceptor axon pathfinding in Drosophila. *Cell*
594 **101**:283–294. doi:10.1016/S0092-8674(00)80838-7
595 Nguyen D, Alavi M V., Kim KY, Kang T, Scott RT, Noh YH, Lindsey JD, Wissinger B, Ellisman MH,
596 Weinreb RN, Perkins GA, Ju WK. 2011. A new vicious cycle involving glutamate excitotoxicity,
597 oxidative stress and mitochondrial dynamics. *Cell Death Dis* **2**. doi:10.1038/cddis.2011.117
598 Nitta Y, Kawai H, Maki R, Osaka J, Hakeda-Suzuki S, Nagai Y, Doubková K, Uehara T, Watanabe K,
599 Kosaki K, Suzuki T, Tavosanis G, Sugie A. 2023. Direct evaluation of neuroaxonal degeneration
600 with the causative genes of neurodegenerative diseases in Drosophila using the automated axon
601 quantification system, MeDUsA . *Hum Mol Genet*. doi:10.1093/hmg/ddac307
602 Olichon A, ElAchouri G, Baricault L, Delettre C, Belenguer P, Lenaers G. 2007. OPA1 alternate splicing
603 uncouples an evolutionary conserved function in mitochondrial fusion from a vertebrate restricted
604 function in apoptosis. *Cell Death Differ* **14**:682–692. doi:10.1038/sj.cdd.4402048
605 Olichon A, Emorine LJ, Descoins E, Pelloquin L, Brichese L, Gas N, Guillou E, Delettre C, Valette A,
606 Hamel CP, Ducommun B, Lenaers G, Belenguer P. 2002. The human dynamin-related protein
607 OPA1 is anchored to the mitochondrial inner membrane facing the inter-membrane space. *FEBS*
608 *Lett* **523**:171–176. doi:10.1016/S0014-5793(02)02985-X
609 Olichon A, Guillou E, Delettre C, Landes T, Arnauné-Pelloquin L, Emorine LJ, Mils V, Daloyau M,

610 Hamel C, Amati-Bonneau P, Bonneau D, Reynier P, Lenaers G, Belenguer P. 2006. Mitochondrial
611 dynamics and disease, OPA1. *Biochim Biophys Acta - Mol Cell Res*.
612 doi:10.1016/j.bbamcr.2006.04.003
613 Poole AC, Thomas RE, Yu S, Vincow ES, Pallanck L. 2010. The mitochondrial fusion-promoting factor
614 mitofusin is a substrate of the PINK1/parkin pathway. *PLoS One* **5**.
615 doi:10.1371/journal.pone.0010054
616 Powell BL, Toomes C, Scott S, Yeung A, Marchbank NJ, Spry PGD, Lumb R, Inglehearn CF, Churchill
617 AJ. 2003. Polymorphisms in OPA1 are associated with normal tension glaucoma. *Mol Vis* **9**:460–
618 464.
619 Rahn JJ, Stackley KD, Chan SSL. 2013. Opa1 Is Required for Proper Mitochondrial Metabolism in Early
620 Development. *PLoS One* **8**. doi:10.1371/journal.pone.0059218
621 Richard M, Doubková K, Nitta Y, Kawai H, Sugie A, Tavosanis G. 2022. A Quantitative Model of
622 Sporadic Axonal Degeneration in the Drosophila Visual System. *J Neurosci* **42**:4937–4952.
623 doi:10.1523/JNEUROSCI.2115-21.2022
624 Rolland SG, Lu Y, David CN, Conradt B. 2009. The BCL-2-like protein CED-9 of C. elegans promotes
625 FZO-1/Mfn1,2- and EAT-3/Opa1-dependent mitochondrial fusion. *J Cell Biol* **186**:525–540.
626 doi:10.1083/jcb.200905070
627 Rubenstein JLR, Brutlag D, Clayton DA. 1977. The mitochondrial DNA of drosophila melanogaster

628 exists in two distinct and stable superhelical forms. *Cell* **12**:471–482. doi:10.1016/0092-
629 8674(77)90123-4
630 Rujiviphat J, Meglei G, Rubinstein JL, McQuibban GA. 2009. Phospholipid association is essential for
631 dynamin-related protein Mgm1 to function in mitochondrial membrane fusion. *J Biol Chem*
632 **284**:28682–28686. doi:10.1074/jbc.M109.044933
633 Sandoval H, Yao CK, Chen K, Jaiswal M, Donti T, Lin YQ, Bayat V, Xiong B, Zhang K, David G,
634 Charng WL, Yamamoto S, Duraine L, Graham BH, Bellen HJ. 2014. Mitochondrial fusion but not
635 fission regulates larval growth and synaptic development through steroid hormone production. *Elife*
636 **3**:1–23. doi:10.7554/eLife.03558
637 Sanes JR, Zipursky SL. 2020. Synaptic Specificity, Recognition Molecules, and Assembly of Neural
638 Circuits. *Cell*. doi:10.1016/j.cell.2020.04.008
639 Sanes JR, Zipursky SL. 2010. Design Principles of Insect and Vertebrate Visual Systems. *Neuron*.
640 doi:10.1016/j.neuron.2010.01.018
641 Sarzi E, Angebault C, Seveno M, Gueguen N, Chaix B, Bielicki G, Boddaert N, Mausset-Bonnefont AL,
642 Cazevieille C, Rigau V, Renou JP, Wang J, Delettre C, Brabet P, Puel JL, Hamel CP, Reynier P,
643 Lenaers G. 2012. The human OPA1delTTAG mutation induces premature age-related systemic
644 neurodegeneration in mouse. *Brain* **135**:3599–3613. doi:10.1093/brain/aws303
645 Sarzi E, Seveno M, Piro-Mégy C, Elzière L, Quilès M, Péquignot M, Müller A, Hamel CP, Lenaers G,

646 Delettre C. 2018. OPA1 gene therapy prevents retinal ganglion cell loss in a Dominant Optic
647 Atrophy mouse model. *Sci Rep* **8**. doi:10.1038/s41598-018-20838-8
648 Schindelin J, Arganda-Carreras I, Frise E, Kaynig V, Longair M, Pietzsch T, Preibisch S, Rueden C,
649 Saalfeld S, Schmid B, Tinevez JY, White DJ, Hartenstein V, Eliceiri K, Tomancak P, Cardona A.
650 2012. Fiji: An open-source platform for biological-image analysis. *Nat Methods*.
651 doi:10.1038/nmeth.2019
652 Shahrestani P, Leung HT, Le PK, Pak WL, Tse S, Ocorr K, Huang T. 2009. Heterozygous mutation of
653 Drosophila Opa1 causes the development of multiple organ abnormalities in an age-dependent and
654 organ-specific manner. *PLoS One* **4**. doi:10.1371/journal.pone.0006867
655 Shimizu S, Mori N, Kishi M, Sugata H, Tsuda A, Kubota N. 2003. A novel mutation in the OPA1 gene in
656 a Japanese patient with optic atrophy. *Am J Ophthalmol* **135**:256–257. doi:10.1016/S0002-
657 9394(02)01929-3
658 Sladen PE, Perdigão PRL, Salsbury G, Novoselova T, van der Spuy J, Chapple JP, Yu-Wai-Man P,
659 Cheetham ME. 2021. CRISPR-Cas9 correction of OPA1 c.1334G>A: p.R445H restores
660 mitochondrial homeostasis in dominant optic atrophy patient-derived iPSCs. *Mol Ther - Nucleic*
661 *Acids* **26**:432–443. doi:10.1016/j.omtn.2021.08.015
662 Spiegel R, Saada A, Flannery PJ, Burté F, Soiferman D, Khayat M, Eisner V, Vladovski E, Taylor RW,
663 Bindoff LA, Shaag A, Mandel H, Schuler-Furman O, Shalev SA, Elpeleg O, Yu-Wai-Man P. 2016.

664 Fatal infantile mitochondrial encephalomyopathy, hypertrophic cardiomyopathy and optic atrophy
665 associated with a homozygous OPA1 mutation. *J Med Genet* **53**:127–131. doi:10.1136/jmedgenet-
666 2015-103361
667 Sugie A, Möhl C, Hakeda-Suzuki S, Matsui H, Suzuki T, Tavosanis G. 2017. Analyzing synaptic
668 modulation of drosophila melanogaster photoreceptors after exposure to prolonged light. *J Vis Exp*
669 **2017**. doi:10.3791/55176
670 Tang S, Le PK, Tse S, Wallace DC, Huang T. 2009. Heterozygous mutation of Opa1 in Drosophila
671 shortens lifespan mediated through increased reactive oxygen species production. *PLoS One* **4**.
672 doi:10.1371/journal.pone.0004492
673 Toomes C, Marchbank NJ, Mackey DA, Craig JE, Newbury-Ecob RA, Bennett CP, Vize CJ, Desai SP,
674 Black GCM, Patel N, Teimory M, Markham AF, Inglehearn CF, Churchill AJ. 2001. Spectrum,
675 frequency and penetrance of OPA1 mutations in dominant optic atrophy. *Hum Mol Genet* **10**:1369–
676 1378. doi:10.1093/hmg/10.13.1369
677 Trevisan T, Pendin D, Montagna A, Bova S, Ghelli AM, Daga A. 2018. Manipulation of Mitochondria
678 Dynamics Reveals Separate Roles for Form and Function in Mitochondria Distribution. *Cell Rep*
679 **23**:1742–1753. doi:10.1016/j.celrep.2018.04.017
680 Tsuyama T, Tsubouchi A, Usui T, Imamura H, Uemura T. 2017. Mitochondrial dysfunction induces
681 dendritic loss via eIF2α phosphorylation. *J Cell Biol* **216**:815–834. doi:10.1083/jcb.201604065

682 Vagnoni A, Bullock SL. 2016. A simple method for imaging axonal transport in aging neurons using the
683 adult Drosophila wing. *Nat Protoc* **11**:1711–1723. doi:10.1038/nprot.2016.112
684 Verny C, Loiseau D, Scherer C, Lejeune P, Chevrollier A, Gueguen N, Guillet V, Dubas F, Reynier P,
685 Amati-Bonneau P, Bonneau D. 2008. Multiple sclerosis-like disorder in OPA1-related autosomal
686 dominant optic atrophy. *Neurology* **70**:1152–1153. doi:10.1212/01.wnl.0000289194.89359.a1
687 Wang JT, Medress ZA, Barres BA. 2012. Axon degeneration: Molecular mechanisms of a self-
688 destruction pathway. *J Cell Biol*. doi:10.1083/jcb.201108111
689 Whitworth AJ, Lee JR, Ho VMW, Flick R, Chowdhury R, McQuibban GA. 2008. Rhomboid-7 and
690 HtrA2/Omi act in a common pathway with the Parkinson's disease factors Pink1 and Parkin. *DMM*
691 *Dis Model Mech* **1**:168–174. doi:10.1242/dmm.000109
692 Yang L, Tang H, Lin X, Wu Y, Zeng S, Pan Y, Li Y, Xiang G, Lin YF, Zhuang SM, Song Z, Jiang Y,
693 Liu X. 2020. OPA1-Exon4b Binds to mtDNA D-Loop for Transcriptional and Metabolic
694 Modulation, Independent of Mitochondrial Fusion. *Front Cell Dev Biol* **8**.
695 doi:10.3389/fcell.2020.00180
696 Yarosh W, Monserrate J, Tong JJ, Tse S, Le PK, Nguyen K, Brachmann CB, Wallace DC, Huang T.
697 2008. The molecular mechanisms of OPA1-mediated optic atrophy in Drosophila model and
698 prospects for antioxidant treatment. *PLoS Genet* **4**:0062–0071. doi:10.1371/journal.pgen.0040006
699 Yu-Wai-Man P, Griffiths PG, Gorman GS, Lourenco CM, Wright AF, Auer-Grumbach M, Toscano A,

700 Musumeci O, Valentino ML, Caporali L, Lamperti C, Tallaksen CM, Duffey P, Miller J, Whittaker
701 RG, Baker MR, Jackson MJ, Clarke MP, Dhillon B, Czermin B, Stewart JD, Hudson G, Reynier P,
702 Bonneau D, Marques W, Lenaers G, McFarland R, Taylor RW, Turnbull DM, Votruba M, Zeviani
703 M, Carelli V, Bindoff LA, Horvath R, Amati-Bonneau P, Chinnery PF. 2010a. Multi-system
704 neurological disease is common in patients with OPA1 mutations. *Brain* **133**:771–786.
705 doi:10.1093/brain/awq007

706 Yu-Wai-Man P, Spyropoulos A, Duncan HJ, Guadagno J V., Chinnery PF. 2016. A multiple sclerosis-
707 like disorder in patients with OPA1 mutations. *Ann Clin Transl Neurol* **3**:723–729.
708 doi:10.1002/acn3.323

709 Yu-Wai-Man P, Stewart JD, Hudson G, Andrews RM, Griffiths PG, Birch MK, Chinnery PF. 2010b.
710 OPA1 increases the risk of normal but not high tension glaucoma. *J Med Genet* **47**:120–125.
711 doi:10.1136/jmg.2009.067512

712 Zaninello M, Palikaras K, Naon D, Iwata K, Herkenne S, Quintana-Cabrera R, Semenzato M, Grespi F,
713 Ross-Cisneros FN, Carelli V, Sadun AA, Tavernarakis N, Scorrano L. 2020. Inhibition of
714 autophagy curtails visual loss in a model of autosomal dominant optic atrophy. *Nat Commun* **11**.
715 doi:10.1038/s41467-020-17821-1

716 Zanna C, Ghelli A, Porcelli AM, Karbowski M, Youle RJ, Schimpf S, Wissinger B, Pinti M, Cossarizza
717 A, Vidoni S, Valentino ML, Rugolo M, Carelli V. 2008. OPA1 mutations associated with dominant

718 optic atrophy impair oxidative phosphorylation and mitochondrial fusion. *Brain* **131**:352–367.

719 doi:10.1093/brain/awm335

720

721

722

723

724

725

726

727

728

729

730

731

732

733

734

735

736 ***Figures with the corresponding legend***

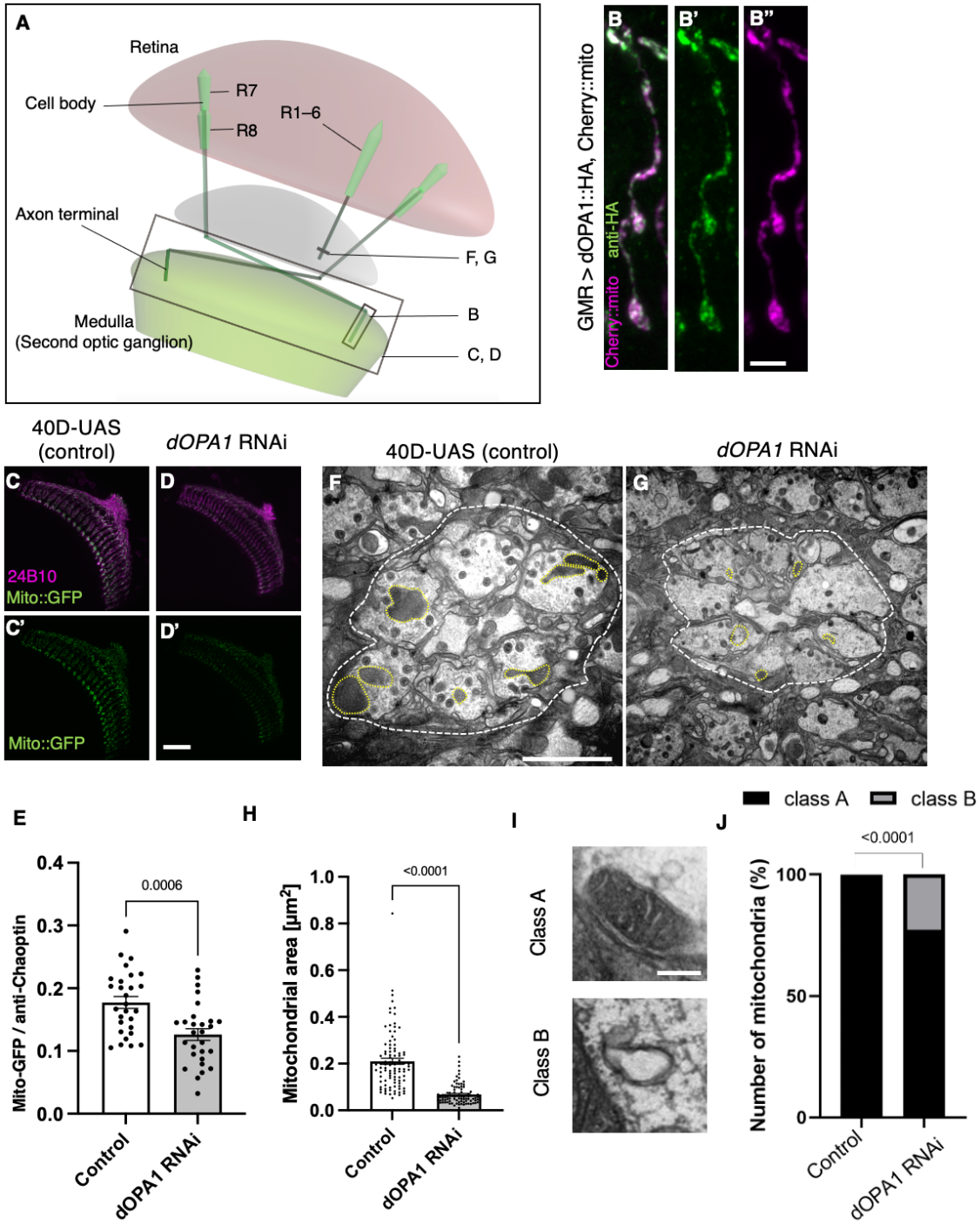

737

738 **Figure 1: Effect of *dOPA1* knockdown on mitochondrial density and size in retinal axons.**

739 (A) Schematic illustration of the *Drosophila* visual system from a dorsal view. (B) Visualization of

740 mitochondria and dOPA1 in a set of R7/8 axons. Mitochondria were visualized using the expression
741 of *mCherry-mito* driven by *GMR-Gal4* (magenta) while HA-tagged dOPA1 was immunostained using
742 the anti-HA antibody (green). Scale bar: 3 μm. (C, D) Representations of mitochondria visualized
743 using the expression of *Mito::GFP* driven by *GMR-Gal4* (green), one day after eclosion. Retinal axons
744 were labeled using the anti-Chaoptin antibody (magenta). Scale bar: 30 μm. (E) Quantification of
745 Mito::GFP intensity. Mito::GFP levels were calculated by dividing the Mito::GFP fluorescence
746 intensity by the anti-Chaoptin signal intensity. Control (n = 28 optic lobes) and *dOPA1* RNAi (n = 28
747 optic lobes). The data are presented as mean ± SEM. (F, G) Electron micrographs of cross sections of
748 the R1–6 retinal axons in the lamina of the Control (F) and d*OPA1* knockdown (G) on the day of
749 eclosion. Yellow circles and white dotted lines indicate mitochondria and a lamina column,
750 respectively. Scale bar: 2 μm. (H) Quantification of the mitochondrial area. Control (n = 96
751 mitochondria) and *dOPA1* RNAi (n = 92 mitochondria). Data are expressed as mean ± SEM. (I)
752 Representative EM images showing mitochondria with a densely packed matrix structure (classified
753 as class A) and collapsed mitochondria (classified as class B). Scale bar: 500 nm. (H) Quantification
754 of the mitochondria classified into class A and class B. Control (n = 96 mitochondria) and *dOPA1*
755 RNAi (n = 92 mitochondria). Data are analyzed by Chi-square test.
756
757

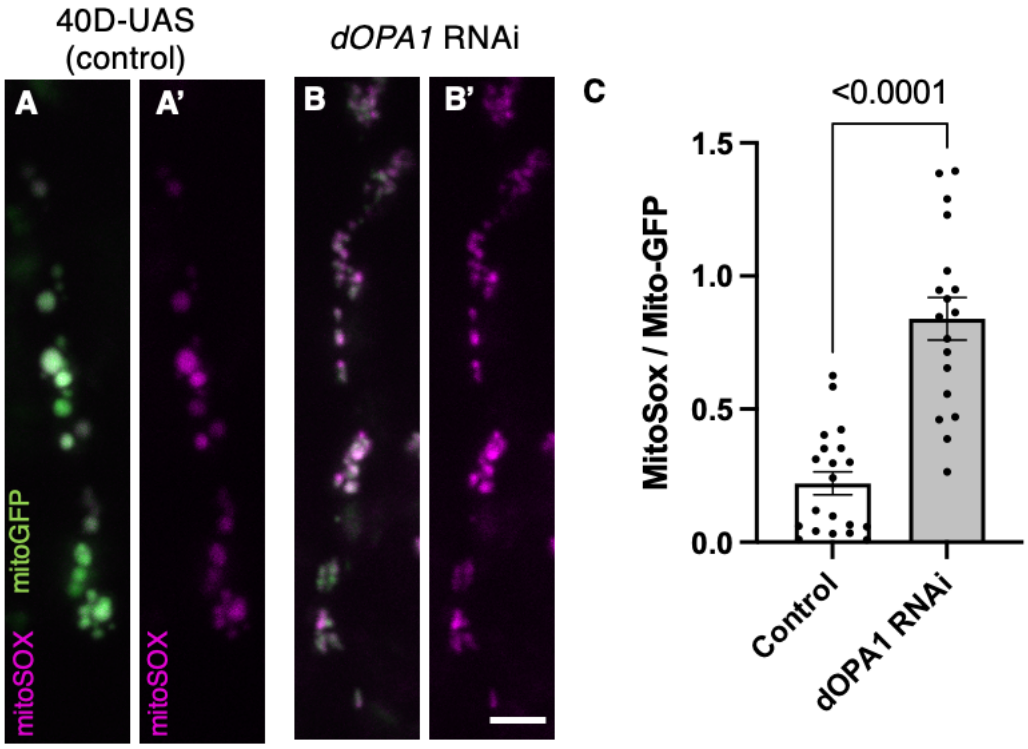

Figure 2. elevated reactive oxygen species levels in the *dOPA1* knockdown.

(A, B) Mitochondrial reactive oxygen species (ROS) levels in a retinal axon visualized using mito-GFP (green) driven by *GMR-Gal4* and MitoSOX (magenta). Representative images of a retinal axon in the Control (A, A') and *dOPA1* knockdown (B, B'). (C) Quantification of ROS levels for each genotype. ROS levels were determined by dividing the fluorescence intensity of MitoSOX by that of mito-GFP. Control (n = 20 optic lobes) and *dOPA1* RNAi (n = 18 optic lobes). Scale bar: 3 µm. Data are presented as mean ± SEM.

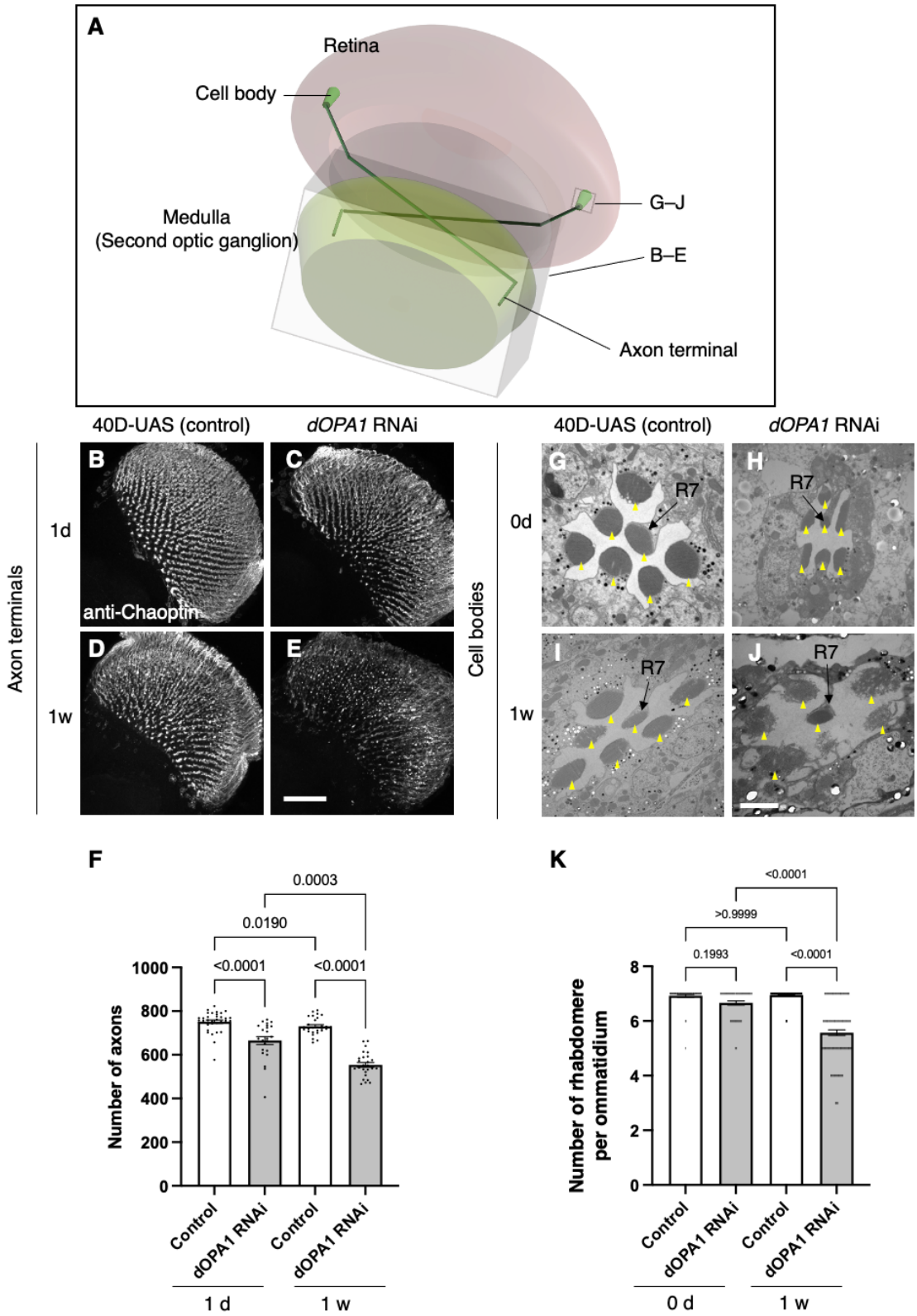

767

768 **Figure 3. Effect of *dOPA1* knockdown on photoreceptor neurodegeneration in *Drosophila*.**

769 Schematic of the visual system in *Drosophila*. A set of R7/8 photoreceptors project their axons to the

770 second optic ganglion medulla. (B–E) All R7 and R8 axon terminals project to the medulla. *dOPA1* in

771 the photoreceptor was knocked down by *GMR-Gal4*. *40D-UAS* was used as a Control to match the

772 number of *UAS* sequences recognized by Gal4. One day after eclosion in Control (B) and *dOPA1*

773 knockdown (C), and one week after in Control (D) and *dOPA1* knockdown €. The retinal axons were

774 stained with anti-Chaoptin, a photoreceptor-specific antibody. Scale bar = 50 μm. (F) Number of axons

775 at each time point in R7 neurons for each situation quantified by MeDUsA. At 1 day of Control (n =

776 34 optic lobes) and *dOPA1* RNAi (n = 23 optic lobes), and at 1 week of Control (n = 28 optic lobes)

777 and *dOPA1* RNAi (n = 26 optic lobes). Data are expressed as mean ± SEM. (G–J) Electron

778 micrographs of cross sections of the photoreceptor cell bodies in the ommatidia of the retina.

779 Rhabdomeres are shown as yellow arrowheads. The day of eclosion in Control **(**G**)** and *dOPA1*

780 knockdown (H), and 1-week-old adults of Control (I) and *dOPA1* knockdown (J). Scale bar = 2 μm.

781 **(**K**)** Quantification of the number of rhabdomeres for each genotype and time point. At 0 day in Control

782 (n = 50 ommatidia) and *dOPA1* RNAi (n = 127 ommatidia), and at 1 week in Control (n = 50

783 ommatidia) and *dOPA1* RNAi (n = 117 ommatidia). Data are expressed as mean ± SEM.

784

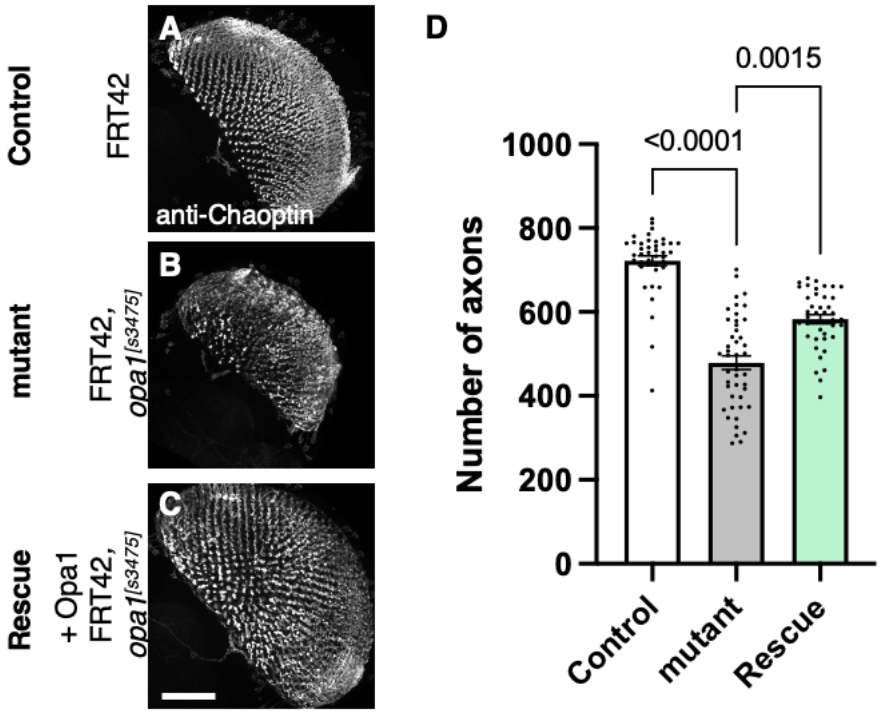

Figure 4. Role of *dOPA1* in the retinal axon according to mutant analysis.

(A–C) Representations of retinal axons labeled with an anti-Chaoptin antibody (gray), one day after eclosion. The images show Control (A), *dOPA1*^{s3475} somatic mosaic flies (B), and *dOPA1*^{s3475} somatic mosaic flies expressing the eye-specific full-length *dOPA1* (C). Scale bar: 50 µm. (D) Quantification of the number of axons for each genotype. Control (n = 41 optic lobes), mutant (n = 45 optic lobes), and rescue (n = 41 optic lobes). The data are presented as mean ± SEM.

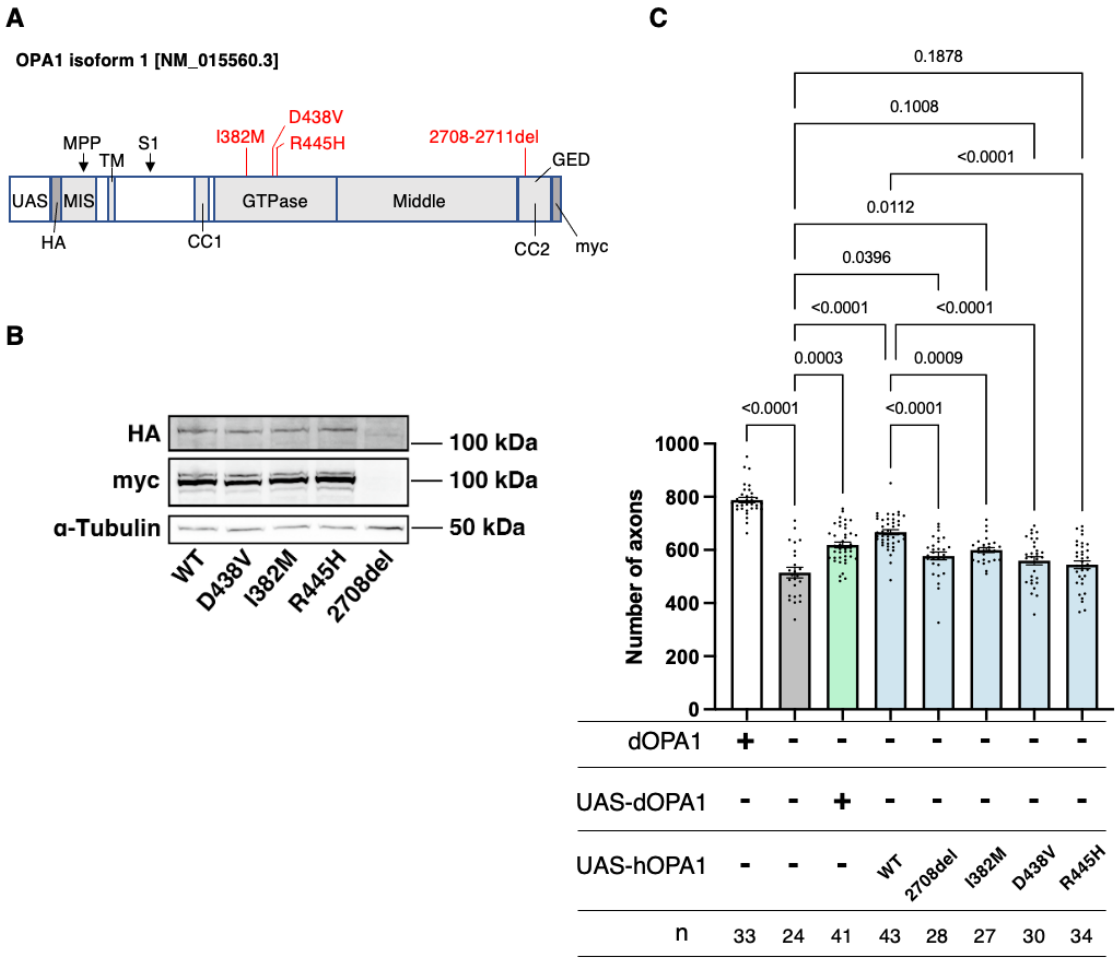

Figure 5. Verification of the pathological significance of disease mutations in *hOPA1*.

(A) Schematic illustration of the *hOPA1* gene construct with HA and myc tags in the UAS-based vector. *hOPA1* includes a mitochondrial import sequence (MIS) cleaved by mitochondrial processing peptidase (MPP), a transmembrane region (TM), a coiled-coil region (CC1), a GTPase domain, a Middle domain, and a GTPase effector domain (GED) containing a coiled-coil region (CC2). The sites of variants (I382M, D438V, R445H, and a deletion from 2708 to 2711) are shown in red. S1 is the site cleaved by OMA1. (B) Western blot analysis to confirm the expression of hOPA1 variants. hOPA1_WT, hOPA1_D438V, hOPA1_I382M, hOPA1_R445H, and hOPA1_2708del were expressed

802 in whole *Drosophila* bodies and detected using anti-HA and anti-myc antibodies. α-Tubulin was used

803 as a loading Control. (C) Rescue experiments were conducted to assess the expression of each *hOPA1*

804 variant, including *dOPA1*, in the retina axons of *dOPA1* mutant somatic clones. The sample size is

805 indicated (n). Data are presented as mean ± SEM.

806

807

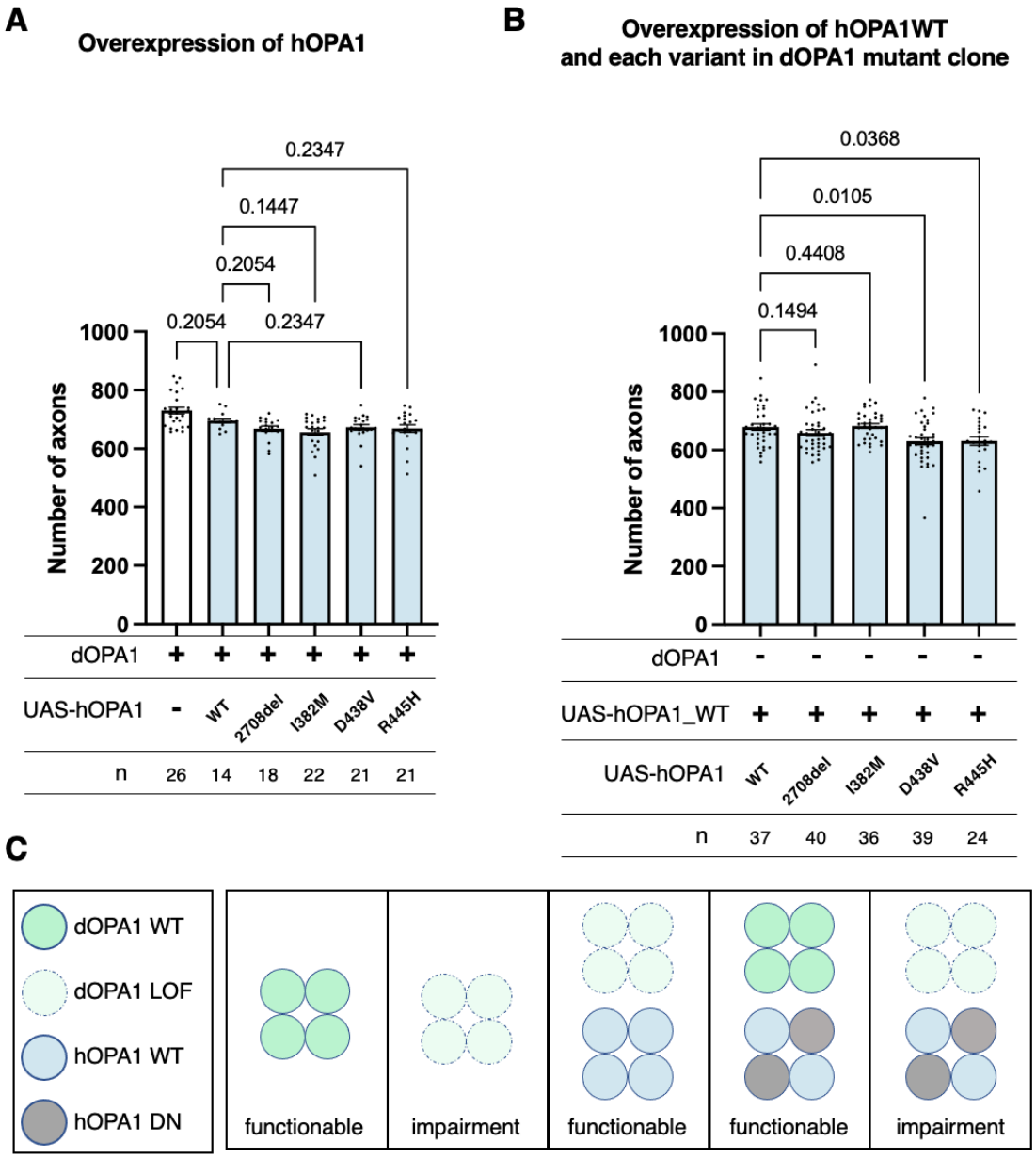

Figure 6. LOF or DN effects of disease mutations in *hOPA1*.

(A) Impact of each human OPA1 variant on the axon number in the optic nerve of *Drosophila* as quantified using MeDUsA. (B) Expression of both *hOPA1* WT and its respective variants was analyzed in photoreceptors lacking *dOPA1*, and the number of axons was quantified using the MeDUsA. The sample size is indicated (n). Data are expressed as mean ± SEM. (C) Schematic representation of

814 interspecies differences in OPA1 interactions and the interchangeability of OPA1 between human and

815 fly.